THE EVOLUTION OF LARGE WAVES IN SHALLOW WATER

VASILIKI KATSARDI & CHRIS SWAN

Department of Civil & Environmental Engineering, Imperial College, London, SW7 2AZ, UK

The evolution of large waves in realistic *JONSWAP* spectra is calculated using the fully nonlinear wave model proposed by Bateman, Swan & Taylor (2001 & 2003). Comparisons between wave fields of varying nonlinearity and between "equivalent" deep and shallow water wave cases confirm that the water depth has a profound influence on the characteristics of large waves in uni-directional seas. In deep water, the evolution of large waves is controlled by linear dispersion. However, as the water depth reduces frequency dispersion is weakened, and the competing process of wave modulation becomes dominant. As a result, the evolution of nonlinear waves in an intermediate water depth (d=15m) is shown to be characterised by a narrowing of the underlying frequency spectrum in which resonant or near-resonant wave interactions create a quasi-regular wave pattern, not previously present in the wave field, and the modulation between closely spaced frequency components, or side-band instabilities, leads to the generation of a large wave event always appearing at the front of an elongated wave group. Calculations involving limiting, or near-limiting, wave events suggest that the largest waves may be characterised by a wave height to water depth ratio of H/d=0.55. This is significantly lower than the established value of H/d=0.78, commonly adopted in engineering design, and appears to be consistent with recent laboratory observations reported by Kamphius (1991b) and Massel (1998).

1. Introduction

This paper concerns the formation of large waves in intermediate and shallow water depths and, in particular, considers whether recent advances in our understanding of how large waves evolve in deep water are appropriate to shallower water depths. In deep water, it is well established that the largest waves do not arise as part of a regular wave train, but occur as transient events in random and directionally spread wave fields due to the focusing of freely propagating wave components. This is the process whereby a large number of wave crests, corresponding to different frequencies and having different directions of propagation, are superimposed at one point in space and time. This produces a large wave crest that rapidly disperses in both space and time.

Historically, these events were investigated using long time-domain simulation, where the input is based upon either linear or second-order random wave theory. However, having appreciated the nature of these focusing events, Tromans *et al.* (1991) built upon earlier work of Lindgren (1970) and Bocotti

(1983) and proposed the so-called *NewWave* model. This describes the expected or most probable shape of a large linear wave of given height as the scaled autocorrelation function of the underlying spectrum and thereby eliminates the need for long time-domain simulations. Comparisons with field data (Jonathan et al., 1994) confirmed the validity of this approach in deep water; its practical significance acknowledged by its inclusion in recent API (American Petroleum Institute) and ISO (International Standards Organisation) guidance notes (Smith & Birkinshaw, 1996). The purpose of the present paper is to examine whether similar procedures can be applied in intermediate and shallow water depths. To resolve this, the evolution of large waves in shallower water is considered and the role of linear dispersion assessed.

2. Wave modelling

Recent advances in wave modelling allow fully nonlinear predictions of the evolution of large waves in realistic wave fields, involving a significant spread of wave energy in both frequency and direction. In particular, Bateman, Swan & Taylor (2001) provide a highly efficient wave model in which a spatial description of the water surface elevation, $\eta(x,y)$, and the velocity potential on that surface, $\phi(x,y,\eta)$ are time-marched using the fully nonlinear free-surface boundary conditions coupled with a Taylor series expansion of the Dirichlet – Neumann operator. In a follow-up paper, Bateman, Swan & Taylor (2003) apply a related approach to accurately describe the internal water particle kinematics based on the previous solution for $\eta(x,y)$ and $\phi(x,y,\eta)$. An essential element of both of these wave models lies in their computational efficiency. This is not sought for its own sake, but is an absolute requirement necessary to achieve the very high resolution in both the wave number and the directional domains, without which realistic wave fields cannot be successfully modelled. Taken together these two wave models, hereafter referred to as *BST*, provide a complete solution of highly nonlinear transient wave events arising in irregular or random wave fields, involving significant directional spread. Given that these wave models provide the basis of the present numerical calculations, a brief review is included herein.

With the fluid motion assumed to be irrotational a velocity potential, $\phi(x,y,z,t)$, can be defined so that the velocity vector $\underline{u}=(u,v,w)=\nabla\phi$, where (x,y) defines horizontal plane at the mean water level ($z=0$) and z is defined vertically upwards. If the fluid is assumed to be inviscid and incompressible, the governing fluid equation representing mass continuity is given by Laplace's equation

$$\nabla^2\phi = 0. \qquad (1)$$

This is valid throughout the fluid domain, bounded by a horizontal bed at $z=-d$ and the water surface at $z=\eta(x,y,z)$. If the bed is assumed to be impermeable, it follows that

$$\phi_z = 0 \quad \text{on} \quad z = -d. \tag{2}$$

At the water surface, $z=\eta$, two nonlinear free-surface boundary conditions apply: a kinematic condition which ensures that fluid particles located at the water surface remain there; and a dynamic condition which requires the pressure acting at the water surface to be constant. After some re-arrangement, these conditions can be written as:

$$\eta_t = \phi_z - \eta_x \phi_x - \eta_y \phi_y \,, \tag{3}$$

$$\phi_t = -g\eta - \tfrac{1}{2}[\nabla\phi]^2 \,. \tag{4}$$

Within equations (3) and (4) all the time dependence arises on the left-hand side. Accordingly, given a spatial representation of η and ϕ at some initial time, $t=t_o$, equations (3) and (4) can be time-marched allowing the evolution of the wave field to be calculated for all times.

To optimise the efficiency of the numerical procedures, for the reasons noted above, it is important that the problem is formulated in terms of the surface parameters, η and $\phi_{z=\eta}$. This has two over-riding advantages. First, it provides a dimensional reduction and, second, it allows both η and ϕ to be represented by Fourier services so that the evaluation of the unknown coefficients (a task typically undertaken twice per time step) can be rapidly achieved using fast Fourier transforms. This is fundamental to the success of the scheme since it ensures that the computational effort increases as $N\log_e N$, where N is the number of surface points or twice the number of wave components.

Unfortunately, with ϕ only defined on the water surface the calculation of ϕ_z, necessary for the evaluation of equations (3) and (4), requires the application of a Dirichlet-Neumann operator. This problem was first tackled by Craig & Sulem (1993) for unidirectional waves; with *BST* providing an extension to include the effects of directionality. In both cases a so-called *G-operator* was applied such that

$$(\phi_z)_{z=\eta} = G(\eta)(\phi_{z=\eta}) \,. \tag{5}$$

If the water surface elevation, $\eta(x,y,t)$ is defined by a Fourier series

$$\eta(x,y,t) = \sum_{k=-\infty}^{+\infty} \sum_{l=-\infty}^{+\infty} A_{kl} e^{i(kx+ly)} \,, \tag{6}$$

the corresponding velocity potential, satisfying both (1) and (2) is given by

$$\phi(x,y,z,t) = \sum_{k=-\infty}^{+\infty} \sum_{l=-\infty}^{+\infty} a_{kl} \cosh(K(z+d)) e^{i(kx+ly)} \,, \tag{7}$$

where A_{kl} and a_{kl} are functions of time only, k and l are the wave numbers in the x and y directions respectively and $K = (k^2 + l^2)^{1/2}$. Evaluating (7) on $z = \eta$, it follows that:

$$(\phi)_{z=\eta} = \sum_{k=-\infty}^{+\infty} \sum_{l=-\infty}^{+\infty} a_{kl} K \cosh(K(\eta + d)) e^{i(kx+ky)} \tag{8}$$

and

$$(\phi_z)_{z=\eta} = \sum_{k=-\infty}^{+\infty} \sum_{l=-\infty}^{+\infty} a_{kl} K \sinh(K(\eta + d)) e^{i(kx+ky)}. \tag{9}$$

Comparing equations (8) (9) and (5) it follows that the transformation implied by the G-operator simply involves a "multiplication" by $K \tanh(K(\eta + d))$ for all valves of k, l x and y. To avoid the difficulty of working with a function that contains information in both the wave number domain (k, l) and the physical domain (x,y,z), the hyperbolic terms in equations (8) and (9) are re-written as the Taylor series expansion about $\eta=0$, and the G-operator evaluated at various orders. Full details of this approach are given in *BST*.

With the fundamentals of the model explained, the only difficulty that remains is the specification of the initial conditions. In essence, this process merely involves going back sufficiently far in time, to $t=t_0$, so that the wave field is fully dispersed. With the total wave energy spread across the computational domain, there can be no large isolated wave events and thus both the water surface elevation, $\eta(x,y,t)$, and the velocity potential on the surface, $\phi(x,y,\eta,t)$, can be represented by either a linear solution or a second-order solution based on the analytical model of Sharma & Dean (1981). Although this process appears straightforward, the importance of adequately specifying the initial condition cannot be over-estimated. Further details concerning this essential first step and, in particular, the application of the model to realistic ocean spectra are given in Bateman & Swan (2004).

3. Discussion of Results

The numerical calculations presented within this section concern the evolution of a *JONSWAP* spectrum defined by

$$S_{\eta\eta}(\omega) = \frac{\alpha g^2}{\omega^5} \exp(-\beta \frac{\omega_p^4}{\omega^4}) \gamma^{\exp\left[-\frac{(\omega-\omega_p)^2}{2\omega_p^2\sigma^2}\right]} \tag{10}$$

where α=0.0081, β=1.25, σ=0.07 for $\omega \leq \omega_p$ and 0.09 for $\omega > \omega_p$. In each of the cases presented the peak spectral frequency is given by $\omega_p=0.628$ rad/s, corresponding to a peak period of T_p=10s, and the peak enhancement factor is given by γ=2.5.

To investigate the evolution of large shallow water waves, a large number of numerical runs have been undertaken. In the present paper we will contrast the results relating to three wave trains, of varying nonlinearity, evolving over a flat bed in an intermediate water depth, d=15m. Comparisons between these cases and equivalent deep water cases will demonstrate the extent to which the evolution is dependent upon the water depth.

The first case concerns a very small wave event for which the input amplitude sum, defined by the linear sum of the component wave amplitudes, was set at A=0.05m. With this amplitude sum the wave motion is entirely linear; the evolution of the wave field is governed by linear dispersion; there are no changes to the underlying spectrum; the shape of the largest (focused) wave is identical to the predictions of the *NewWave* model; and the maximum crest elevation corresponds directly to the input amplitude sum, $\eta_{max}=A$. Evidence to this effect is presented on Figure 1. This concerns a spatial description of the water surface elevation, $\eta(x)$, at the time of the focal event and contrasts the results of the *BST* with the *NewWave* predictions for both the deep and intermediate depth cases.

The results presented on Figure 1 were based on input conditions specified at t_0=-850s, or 85 peak periods prior to the focal event. Given the linearity of these wave fields, calculations of this duration were clearly unnecessary. Nevertheless, it ensures that they are consistent with the subsequent nonlinear calculations, and also provides further validation of the *BST* model which had not previously been applied in intermediate water depths. The evolution of the linear wave field in intermediate depth is further considered in Figure 2. This provides ten spatial profiles, $\eta(x)$, at specific times throughout the evolution of the wave field, -850$s \le t \le$ 0s. Although not shown, the numerical predictions of *BST* are identical to the results of a linear random wave theory (*LRWT*) based on the amplitude and phasing of the initial wave components, at t=-850s. Furthermore, comparisons between the equivalent linear cases in deep and intermediate water depth are very similar. Indeed, the only difference is that with the reduction in water depth, the effectiveness of linear dispersion is reduced, and consequently the compression of the wave group as it evolves toward the focal event is less rapid. Nevertheless, it is clear in Figure 2 that the evolution of the wave group is such that it becomes progressively more compact, giving higher local energy densities and hence larger maximum crest elevations.

Figures 3 and 4 provide a similar sequence of wave profiles, $\eta(x)$, describing the evolution of a nonlinear wave field (A=5m) in deep and intermediate water depths. In the deep water case (Figure 3) the evolution is consistent with expectations: the wave group is widely dispersed at t=-850s and becomes progressively more compact as the focal event is approached.

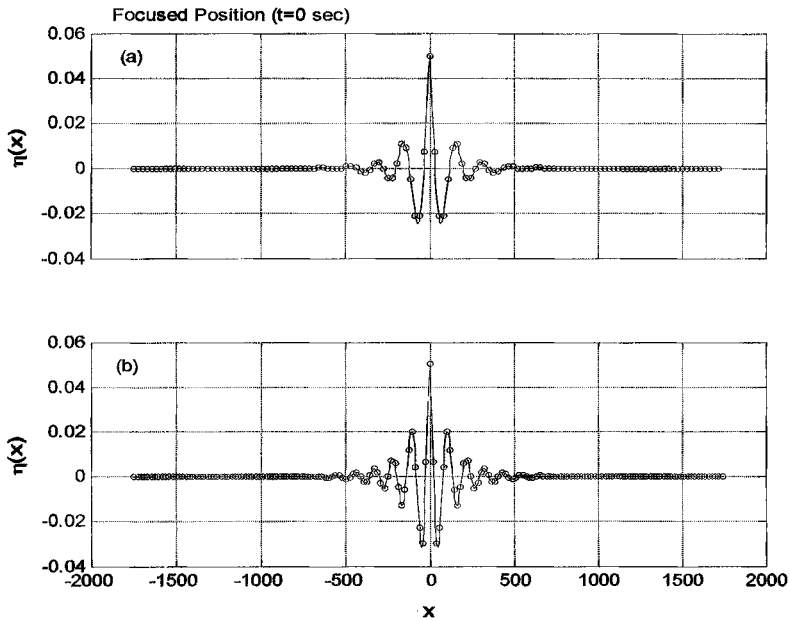

Figure 1. Focused events for (a) Deep water and (b) Intermediate water depth (d=15m). Thin black line: *LRWT* and o o *BST* model.

Although the largest wave event occurs prior to the linearly predicted focus (at t=-19.2s), it is clear that there has been a significant convergence of energy and, as a result, a large crest elevation arises. The nature of the deep water focal event is further considered in Figures 5a and 5b: the former describing the amplitude spectrum, $a_n(k)$, at the time of the largest wave event; while the latter contrasts the nonlinear results of *BST* with the linear predications (*LRWT*) based upon the initial input conditions (t=-850s). It is clear from these figures that the nonlinear effects are significant. In particular, there is a local broadening of the spectrum of the freely propagating wave components, with significant energy transferred to the higher frequencies. This leads to an increase in the local amplitude sum and hence large maximum crest elevations. Furthermore, there are some local changes to the phasing of the wave components such that the largest wave is no longer perfectly focused (Figure 5b). A full discussion of these points is given by Johannessen & Swan (2003) and Gibson & Swan (2004). Although these nonlinear effects are obviously important, it is also clear from Figure 3 that they occur in addition to the domi nant effects of linear dispersion. As a result, the *NewWave* model is largely correct but may significantly underestimate the maximum crest elevation, largely due to the changes in the underlying spectrum (Figure 5a).

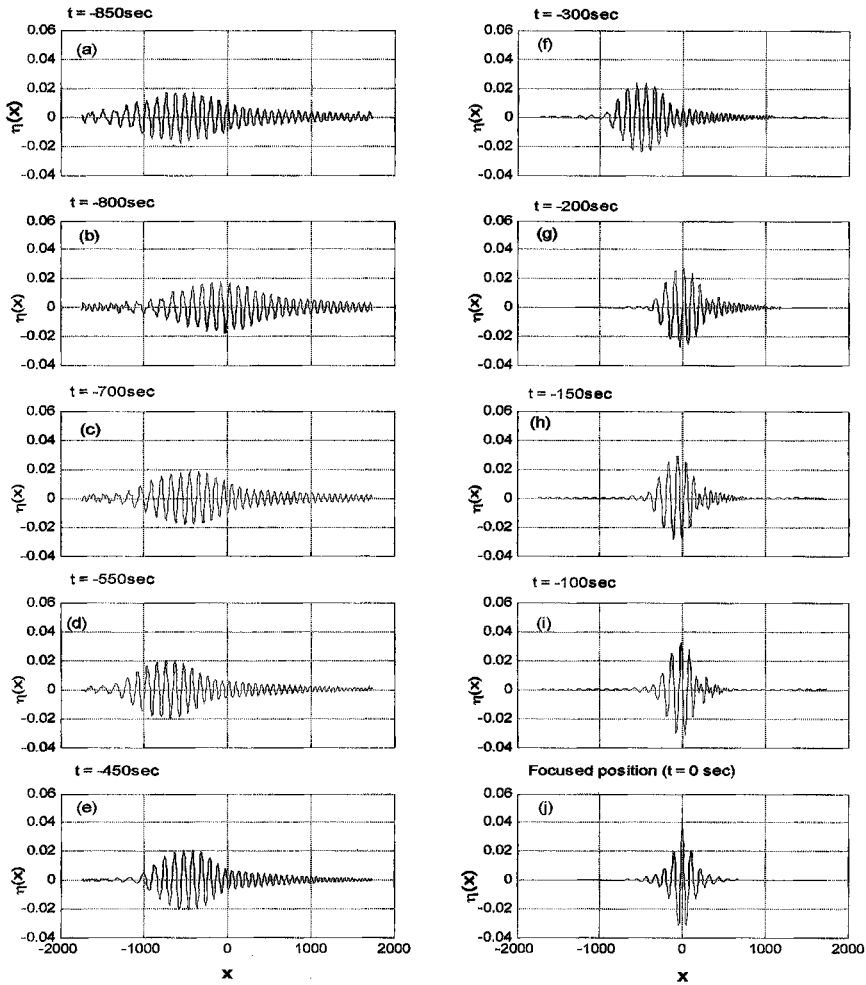

Figure 2. Evolution of a linear wave train in shallow water based on the *BST* model, (A=0.05m).

In contrast, the evolution of the nonlinear wave train is an intermediate water depth (Figure 4) appears fundamentally different from that driven by linear dispersion (Figure 2). In particular, Figure 4 suggests that wave modulation rather than dispersive focusing becomes the driving mechanism. Indeed, these results suggest that from a very early stage (t=-450s) resonant or near-resonant interactions create a quasi-regular wave pattern, not previously present in the wave field, and that modulation between closely spaced frequency components,

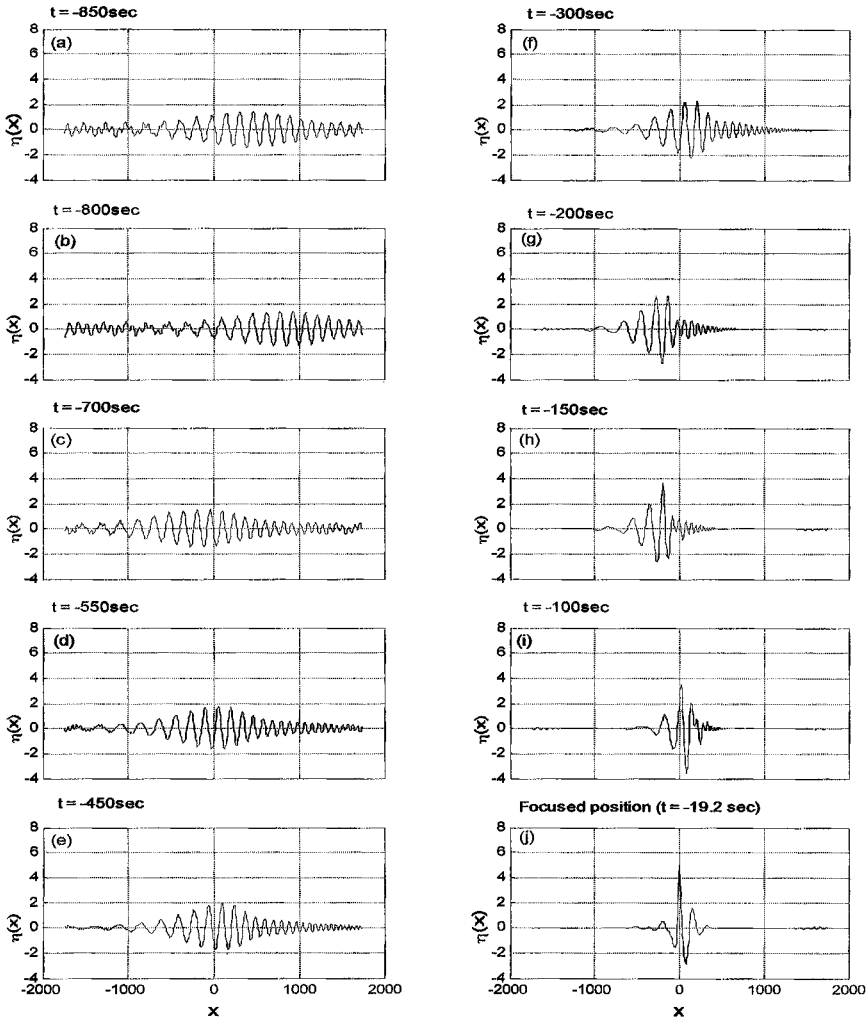

Figure 3. Evolution of a nonlinear wave train in deep water, (A=5m).

or side-band instabilities, lead to the generation of a large wave event always appearing at the front of an elongated wave group. This view is supported by the fact that over the final 450 seconds (or 45 peak periods) the wave group shows almost no evolution and, certainly, no evidence that the group is becoming progressively more compact.

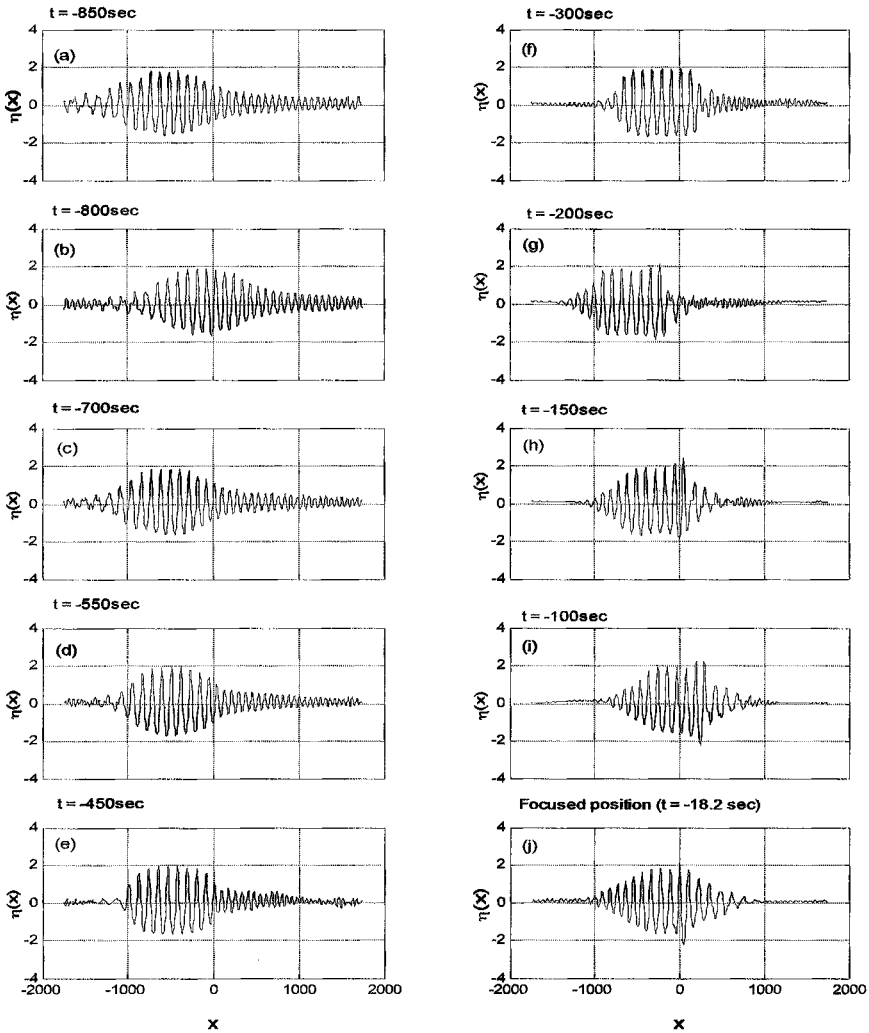

Figure 4. Evolution of a nonlinear wave train in shallow water, (A=5m).

Further evidence of these changes is provided in Figures 5c and 5d. The former indicates that whilst there is clear evidence of the growth of both frequency-sum and frequency-difference terms, corresponding to the well known second-order terms, (Longuet-Higgins and Stewart, 1960), there is an overall reduction in the spectral bandwidth. This is opposite to that which occurs in deep water and produces a reduction in the linear amplitude sum. This effect, together with the absence of energy focusing due to linear dispersion, explains why the

largest crest elevation is significantly smaller than the focusing event predicted by linear theory (figure 5d).

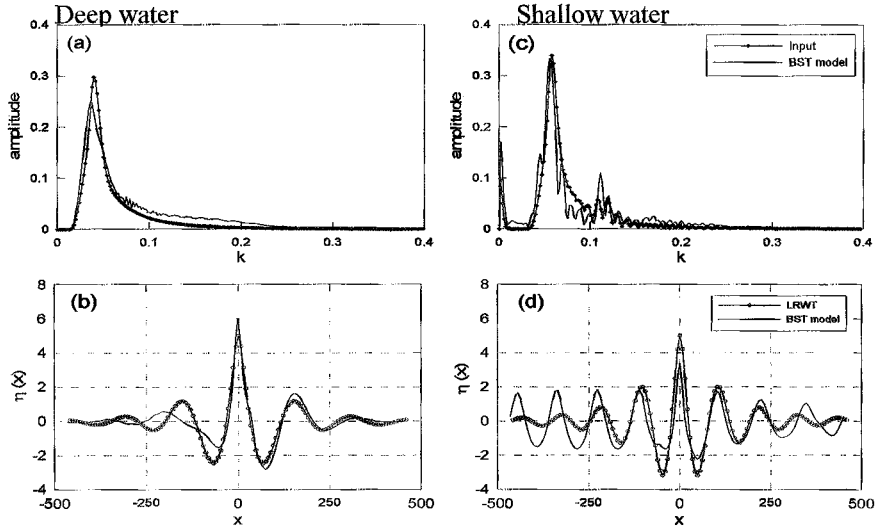

Figure 5. Evolution of spectra and comparisons with linear theory for deep and shallow water.

4. Practical Implications and Concluding Remarks

Having demonstrated that the evolution of large waves in water of intermediate depth is fundamentally different from both the evolution of "equivalent" deep water waves and from the predications of the linear *NewWave* model, it is instructive to consider how the numerical calculations of *BST* compare to typical design wave solutions based on depth-limited wave heights. Although *BST* is not able to model over-turning waves, the model has been successfully compared to laboratory measurements of very steep waves at the limit of wave breaking. Indeed, the latter were within 2% (in terms of the input amplitude sum) at which incipient wave breaking was first observed in the laboratory (Johannesson & Swan, 2001). More importantly, the collapse of the numerical model is characterised by significant, rapid and non-reversible transfers of energy to the very high frequencies, immediately preceding the point at which the laboratory tests indicted that wave breaking occurred. Whilst this does not represent satisfactory grounds to predict the onset of wave breaking (this can only be achieved by evidence of over-turning), it does represent a pre-curser to wave breaking and, as such, provides a reasonable basis on which to estimate a limiting or near-limiting wave height.

In the present intermediate depth case, the largest input amplitude sum that could be applied without evidence of wave breaking was A=9.5m. The evolution of this wave field is described in Figure 6. The format of this figure is similar to those considered previously and, once again, for t>-450s a truncated, quasi-

regular, wave train rapidly evolves. This exhibits very little subsequent evolution until a modulation-type instability leads to the rapid growth of a large wave crest at the front of the group. Comparisons between this maximum crest elevation and a *NewWave* event based on the input *JONSWAP* spectrum and scaled to the traditional depth-limiting criteria, H/d=0.78, are provided on Figure 7. These confirm the importance of the nonlinear evolution of a wave field. Indeed, further comparisons involving a wide range of uni-directional wave spectra suggest that the limiting criteria may be closer to H/d=0.55. Whilst this is clearly significantly lower than the value of H/d=0.78 commonly adopted in engineering design, it is consistent with observations reported by Kamphius (1991b) and Massel (1998).

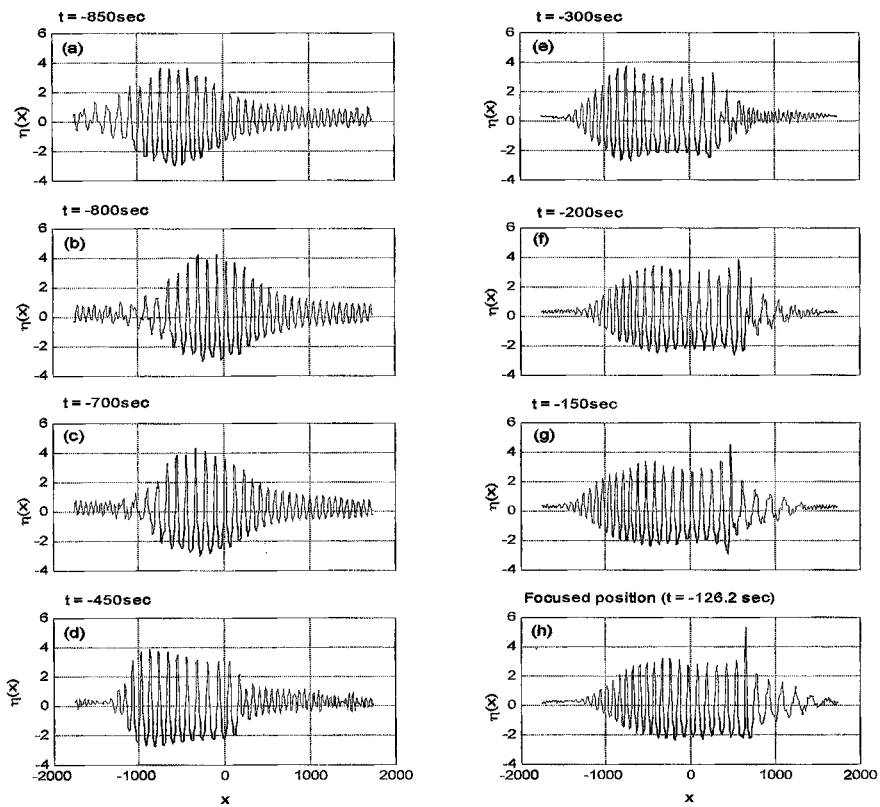

Figure 6: Evolution of the limiting wave train in shallow water, (A=9.5m).

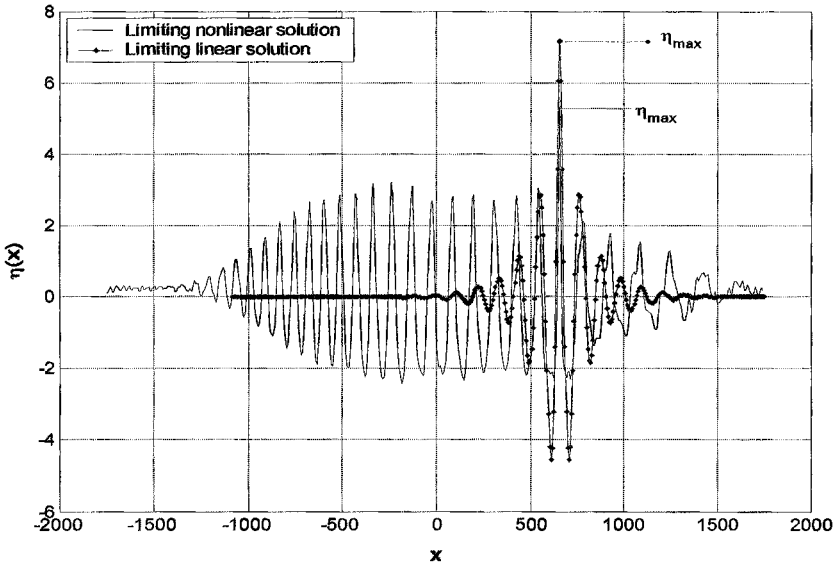

Figure 7: Limiting waves in water of intermediate depth.

References

Bateman, W.J.D., Swan, C. and Taylor, P.H., 2001. On the efficient numerical simulation of directionally spread surface water waves. J.Comp. Physics, 174, 277-305.

Bateman, W.J.D., Swan, C. and Taylor, P.H., 2003. On the calculation of the water particle kinematics arising in a directionally spread wavefield. J.Comp. Physics, 186, 70-92.

Bateman, W.J.D. and Swan, C., 2004. Realistic Descriptions of Extreme Ocean Waves. Part I: The application of recent advances in wave modelling. Submitted to: Applied Ocean Research.

Bocotti, P., 1983. Some new results on statistical properties of wind waves. Appl. Ocean Res., 5, 134-140.

Craig, W. and Sulem, C., 1993. Numerical simulation of gravity waves. J. of Comp. Phys. 108, 73-83.

Gibson, R. and Swan, C., 2004. The evolution of large ocean waves: the role of local and rapid spectral changes. Submitted to: Proc. R. Soc. London.

Lindgren, G., 1970, Some properties of a normal process near a local maximum. Ann. Math. Stat., 41, No.6, 1870-1883.

Johannessen, T.B. and Swan, C., 2001. A laboratory study of the focusing of transient and directionally spread water surface. Proc. R. Soc. London, Ser. A, 457, 971-1006.

Johannessen, T.B. and Swan, C., 2003. On the nonlinear dynamics of wave groups produced by the focusing of surface-water waves, Proc. R. Soc. London, Ser. A, 459, 1021-1052.

Jonathan, P., Taylor, P. H. and Tromans, P.S., 1994. Storm waves in the northern sea. Proceedings of Conference on the Behaviour of Offshore Structures, BOSS94.

Kamphius, J.W., 1991b. Incipient wave breaking. Coastal Eng., 15, 185-203.

Lindgren, G., 1970, Some properties of a normal process near a local maximum. Ann. Math. Stat., 41, No.6, 1870-1883.

Longuet-Higgings, M.S., and Stewart, R.W., 1960. Changes in the form of short gravity waves on long waves and tidal currents. J. Fluid Mech., 8, 565-583.

Massel, S. R., 1998. The limiting wave height in wind-induced wave trains. Ocean Eng, 25, 735-752.

Sharma, J.N. and Dean, R.G., 1981. Second-order directional seas and associated wave forces. Society of Petroleum Eng. J. , 4, 129-140.

Smith, D. and Birkenshaw, M., 1996. ISO(draft) Offshore design codes: wave loading requirements. Trans. Inst. Marine Engs., 108, 89 -96.

Tromans, P.S., Anaturk, A.R. and Hagemeijer, P., 1991. A new model for the kinematics of large ocean waves- application as a design wave, Proc. 1st Int. Conf. Offshore & Polar Engng., UK. 3, 64-71